University of Strathclyde

Department of Naval Architecture, Ocean and Marine Engineering

A study on the efficient numerical analysis for the prediction of full-scale propeller performance using CFD

Kwanwoo Kim

A thesis presented in fulfilment of the requirements for the degree of Master of Philosophy

2022

Acknowledgements

One year of Glasgow life was an unforgettable period of my life. It was my first living in a foreign country, and I cannot forget the memory of the world stopped due to the epidemic of Corona. However, my life in Glasgow before Corona was as varied as the weather in Scotland. Living in a strange place was not easy, but thanks to the good people around me, I could get along.

First of all, thank you to my supervisor, Professor Mehmet Atlar. He always asked if it was going well, and even in the corona pandemic situation, he did not stop paying attention to his disciples. Also, whenever I asked for feedback on the paper, he did his best to help. This has been a tremendous aid to my research.

Thanks also to Dr Yigit Kemal Demirel, my second supervisor. His encouragement and advice gave me the strength to move on. I am deeply grateful to Dr Soonseok Song as well. From adapting to the UK to write my graduation thesis, my entire life in the UK was finished thanks to his help. Likewise, I would like to express my gratitude to Dr Byongug Jeong and Injun Yang, studying PhD. I am also grateful to the people who came with me from Korea and especially to Changbeom Kim, Wookjae Lee, Yunho Jang, Seongjae Jeon, and Seol Nam.

Contents

List of Figures

List of Tables

Abstract

In Computational Fluid Dynamics (CFD) simulations, limited number of full-scale studies with ship propellers have been conducted due to the limitation of computational resources and computation time. There are two methods for efficient full-scale numerical analysis; (1) a method of using large non-dimensional wall-normal distances (y +) and (2) a method of applying a virtual fluid at a model scale. However, there are lack of study on the validity of using large y+ in full-scale propeller simulations and applying virtual fluids. Thus, the aim of this study is to investigate the effect of different wall y+ values in a real fluid and the virtual fluid concept to predict full-scale propeller performance using CFD. For these investigations, the commercial CFD tool, STAR-CCM+, was used to predict the propeller open water (POW) performance of the KRISO benchmark propeller (KP505) in model and full-scale. The results presented include the pressures, friction, streamlines, and tip vortex formation characteristics. The findings of this research study support the use of a small value of wall y+ (i.e., y+<1) for the model scale simulations, but the effect of the wall y+ is negligible in full-scale. This study also demonstrates that the similarity requirements for the advance coefficient and Reynolds number could be satisfied simultaneously in full-scale by using the virtual fluid properties without any need to conduct more computationally demanding full-scale simulations with real fluid.

1. Introduction

1.1. Introduction

This chapter introduces the general perspectives of the subjects covered in this MPhil thesis, presents the motivations of the study, defines the aim and objectives of the study, and finally outlines the structure of the thesis.

1.2. General perspectives

The full-scale performance of a ship usually can be estimated based on model scale predictions, which largely rely on empirical relationships that require accumulated knowledge, experience, and many correction factors, and expensive physical model tests. Thus, a recent and attractive alternative approach for this purpose is to simulate the ship performance in full-scale by using Computational Fluid Dynamics (CFD) methods. However, full-scale simulation of ships has not been adequately studied because of the requirements for large computational resources and time.

Some studies have been conducted on the effect of the Reynolds number in various full-scale performance predictions using viscous solvers. For example, Yang et al. (2010) compared the wake of a model ship and a full-scale ship using CFD. Jasak et al. (2019) studied the sensitivity of the grid size selection for a full-scale ship in a self-propulsion state. Castro et al. (2011) used a discretized propeller to perform a full-scale self-propulsion analysis. Kim et al. (2020) compared two extrapolation methods using the result of a full-scale simulation for predicting the resistance of an air lubrication system.

In CFD applications, the flow near the wall is affected by the values of the non-dimensional wall-normal distance (y+), so the selection of accurate y+ values is critical (ITTC, 2011). High wall y+ values (>30) have been used in the full-scale simulations to avoid an increased grid size since smaller values of wall y+ require high computing performance. Recently, however, improved computing performance may allow lower values for wall y+ in full-scale. Nevertheless, studies using low values of wall y+ in full-scale have been limited, so it is beneficial to study CFD simulations for ship performance by using low wall y+ values in full-scale simulations.

The propulsion performance of a ship depends on the performance of its propeller to overcome the total hull resistance. Many experiments and numerical analyses have been carried out to estimate the propeller performance and understand the physical phenomena involved in propeller flow. Felli et al. (2011) conducted experiments to study how the propeller wake develops in transition and far-field regions. Paik (2003) studied the hydrodynamic characteristics of a propeller operating beneath a free surface. It was shown that the hydrodynamic characteristics of a propeller operating near the free surface could be changed depending on the submergence depth, advance coefficient, and size of the model propeller.

Kawamura et al. (2012) conducted a numerical simulation of a propeller boss cap fin with a different scale. Silvestre et al. (2015) measured the propeller performance at a low Reynolds number. The propeller performance was mainly affected as the Reynolds number increased. Song et al. (2019) conducted simulations to predict the effect of biofouling on a full-scale propeller and the hull.

For ship model tests involving propellers, the advance coefficient similarity is essential to extrapolate the model test data to the full-scale. In order to achieve this similarity law, the advance velocity and/or rotational speed terms to match the full-scale torque or thrust. However, it is impossible to match the advance coefficient and Reynolds number for the model and full-scale propeller at the same time.

If the scale is determined to conduct the model test, one of the easiest variables to change is advance velocity. However, in CFD, a virtual environment can be generated. For example, a virtual fluid with virtual properties can be created numerically. If there is virtual fluid in the model scale, both similarities can be matched at the same time.

Theoretically, when the Reynolds similarity requirement is satisfied, the viscosity phenomena should be the same. However, limited study on this approach has been reported. Sezen et al. (2019) introduced a virtual fluid and performed numerical analysis on the DTMB 5512 ship at the model and full scales. Zhao et al. (2015) studied numerical analysis using virtual fluids for the bulk carrier ships with ESD, and it was confirmed that similar results were produced regardless of the scale. However, a study on a complex application of scale for the effect of varying y+ and that of virtual fluid on a propeller's flow action has not been conducted. An advantage of using virtual fluid is that full-scale simulation should not be needed. Just simulations at the model scale will suffice using the virtual fluid property. This process will save a considerable amount of computational time and resources. For all these reasons, the effect of virtual fluid should be studied.

Thus, as tackled in the present study, it will be most appropriate to investigate the effect of different wall y+ values and the use of the virtual fluid concept on propeller flow modelling. This would preferably be done to predict the propeller open water (POW) performance by using commercial CFD code and validated with available experimental data. This will help to make further progress in obtaining more accurate, efficient, and cost-effective ways of predicting a ship's performance in full-scale.

Therefore, the aim of this study was set to investigate the effect of different wall y+ values in a real fluid and the virtual fluid concept to predict full-scale propeller performance using CFD. For these investigations, the commercial CFD tool, STAR-CCM+, was used to predict the propeller open water (POW) performance of the KRISO benchmark propeller (KP505) in a model and full-scale.

1.3. Motivations

Before detailing the specific objectives of this study, an overview of the general motivations is presented in this section.

- There have been several studies using CFD to investigate various values of wall y+ at full-scale. However, it is necessary to study the very small wall y+ values. It is possible to analyse the influence of the flow characteristics and performance characteristics around the propeller according to the varying wall y+. This could be helpful to predict full-scale performance of the marine propeller.

- There are only a few studies on the use of virtual fluids in CFD simulations. The use of virtual fluids could help predict full-scale performance. However, as far as the author is concerned, there are no studies on marine propellers using virtual fluids. This gap can be filled by performing a CFD simulation.

- There have been many studies on the perturbation of flow around the propeller according to the advanced coefficient. However, as a study for further understanding, the relationship between the advanced ratio and wall y+ can be investigated. This study can be useful in predicting propeller performance and flow characteristics.

1.4. Research aim and objectives

Based on the motivations given in the previous section the main aim of this thesis is to develop computational techniques to investigate the effect of wall y+ and the validity of using virtual fluid on the model scale and full-scale marine propeller.

In order to achieve the above aim, the following objectives are specified:

- Objective 1: To conduct a literature survey for the background knowledge and theory in the effect of wall y+ and virtual fluid on marine propellers (Chapter 2), helping the author effectively use and apply the CFD method to achieve the aim and objectives of this thesis.

- Objective 2: To develop a CFD model to conduct an analysis of the effect of wall y+ and virtual fluid on the model and full-scale propeller (Chapter 3).

- Objective 3: To validate using a CFD model to predict the effect of the wall y+ and virtual fluid on the propeller by comparing the CFD results with the experimental result obtained from POW test (Chapter 4).

- Objective 4: To perform CFD simulations of different fluid types in different scales and advanced coefficients to investigate the effect of wall y+ and virtual fluid on the flow action of marine propellers (Chapter 5).

1.5. Structure of the thesis

The above objectives are achieved in the six chapters of the thesis structured as defined below following this introductory Chapter 1:

Chapter 2 provides a comprehensive review of the literature on related topics, including a high-level understanding and theory of marine propellers, theoretical information on the CFD scheme used in this paper.

Chapter 3 describes the general methodology used in this paper.

Chapter 4 presents the verification of CFD simulations for the validation of CFD results. POW tests were performed in a towing tank for various advance coefficients.

The experimental results were compared with the CFD results for the selected propeller.

Chapter 5 provides the results of the CFD simulations. The characteristics of fluid types, pressure distributions, friction distributions, and flow characteristics around the blade surface were compared for various y+ values, scales, and advance coefficients.

Finally, Chapter 6 presents a comprehensive summary of this dissertation, including research goals, achievements, main conclusions, and future recommendations.

1.6. Chapter summary

The general background, the motivations of this study, the aim and objectives, and the structure of the thesis have been introduced in this chapter.

2. Literature review

2.1. Introduction

An extensive literature and theory survey were conducted in the relevant field to justify the aim of this study.

In section 2.2, a brief review of the marine propeller is presented, including the similarity law and the method of propeller experiments. Section 2.3 reviews the theoretical characteristics of the flow near the wall. Finally, numerical analysis techniques and equations used in the thesis are described in section 2.8.

2.2. Marine propeller

2.2.1. Marine propeller

A propeller is one of the most common propulsion system for ships. Typically, it has 3 to 5 blades, and the number of blades is determined by the vibration frequency of the hull and propulsion shaft. The boss-to-diameter ratio is usually 0.18 to 0.30, and the blade area ratio is determined to meet the cavitation requirements condition. Significant size skews can be applied to reduce propeller excitation force and slightly increase diameter and efficiency. Modifications including tip rake (Andersen, 1999; Dang, 2004) and end plate (Dyne, 2005) can improve the performance of the basic wing. Special application examples of general propellers include super-cavity propellers and surface-piercing propellers for high-speed ships used in situations where cavitation is inevitable. Other types of propellers include Controllable Pitch Propellers, Ducted Propellers, Contra-Rotating Propellers, and Tandem Propellers.

All propulsion mechanisms operate on the principle of imparting momentum to the 'working fluid' according to Newton's law of motion described as follows:

(a) The external acting force is the same as the rate of change of momentum.
(b) Action and reaction are of the same magnitude and opposite directions.

That is, the force required to change the momentum of the working fluid appears as a reaction to the propulsion mechanism, and this becomes the thrust generated by the mechanism. Assuming that the velocity of the fluid passing through the thruster is accelerated from V_1 to V_2 by the action of the propulsion mechanism and the mass passing through the device per unit time is $\dot{m}$, the generated thrust (T) is as follows.

$$T = \dot{m}(V_2 - V_1) \tag{2.1}$$

The general characteristics of any propeller are basically shown in Figure 2.1. The thrust formula (Equation 2.1) shows that T converges to zero when V_1 approaches V_2. That is, when the ratio V_1/V_2 of the forward velocity V_1 to the ejection velocity V_2 increases, the thrust decreases. Two extreme cases can be considered:

(a) In the case of $V_1 = V_2$, the thrust is zero. Therefore, the output is also 0. In this condition, since a little input power is required due to viscous loss, the $\eta = 0$.
(b) In the case of $V_1 = 0$, although the thruster generates the maximum thrust, $\eta = 0$ since the output $TV_1 = 0$.

At any value of V_1/V_2 between these two extreme cases, η becomes maximum. Therefore, it is desirable to design the propulsion mechanism to operate close to this condition for maximum efficiency.

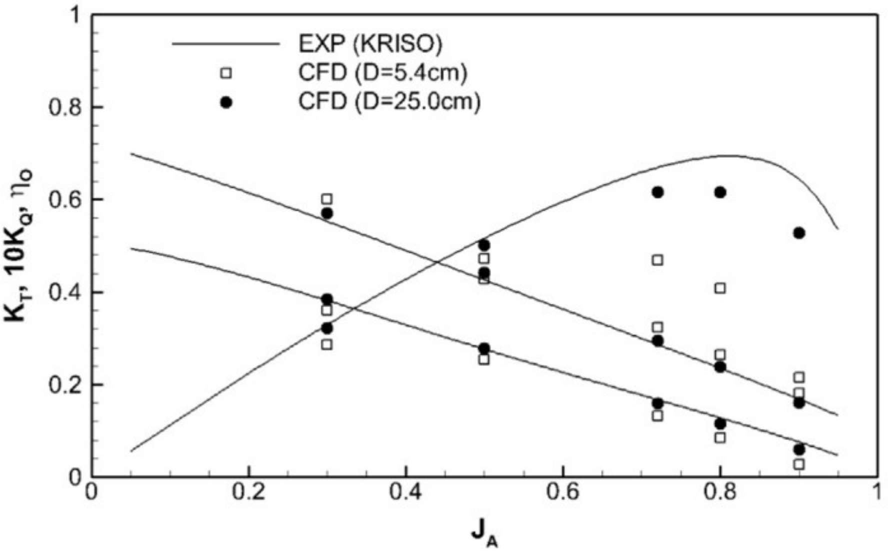

Figure 2.1 The Propeller Open Water (POW) curve, adapted from Paik (2017)

2.2.2. Similarity law

Several combinations of dimensionless coefficients are used in propeller design work. The quantity and dimension related to these coefficients are as follows.

Table 2.1 Physical quantity and dimension for propeller coefficient

Thrust	T	$\frac{ML}{T^2}$
Torque	Q	$\frac{ML^2}{T^2}$
Revolutions Per Second (RPS)	n	$\frac{1}{T}$
Advance speed	V	$\frac{L}{T}$
Diameter	D	L
Density	ρ	$\frac{M}{L^3}$

According to the dimensional analysis method, the relationship between physical quantities is expressed as follows.

$$\text{Thrust: } f(T, D, v, n,\ \rho) \tag{2.2}$$

$$\text{Torque: } f(Q, D, V, n, \rho) \tag{2.3}$$

here, Advance coefficient and thrust, advance coefficient, and torque can each be expressed in two ways.

$$f_1\left[\left(\frac{T}{\rho n^2 D^4}\right),\left(\frac{V}{nD}\right)\right]=0 \tag{2.4}$$

$$f_2\left[\left(\frac{Q}{\rho n^2 D^5}\right),\left(\frac{V}{nD}\right)\right]=0 \tag{2.5}$$

$$f_3\left[\left(\frac{T}{\rho V^2 D^2}\right),\left(\frac{V}{nD}\right)\right]=0 \tag{2.6}$$

$$f_4\left[\left(\frac{Q}{\rho V^2 D^3}\right),\left(\frac{V}{nD}\right)\right]=0 \tag{2.7}$$

The following expressions are commonly used.

$$K_T=\frac{T}{\rho n^2 D^4}, K_Q=\frac{Q}{\rho n^2 D^5}, J=\frac{V}{nD} \tag{2.8}$$

$$C_T=\frac{T}{\rho V^2 D^4}, C_Q=\frac{Q}{\rho V^2 D^3}, J=\frac{V}{nD} \tag{2.9}$$

2.2.3. Expression of propeller data

For most purposes, the preferred method is K_T, K_Q and J (Equation 2.8). C_T, C_Q, and J methods have the disadvantage that C_T and C_Q become infinite when $V -> 0$, so C_T and C_Q are useless in a low-speed example towing tank test and become meaningless under the condition of $V = 0$ bollard pull.

Since the size of $10K_Q$ is roughly similar to K_T, K_T and $10K_Q$ are shown together. Propeller efficiency is determined as follows.

$$\eta_0=\frac{TV_a}{2\pi nQ} \tag{2.10}$$

This basic formula can be written for dimensionless coefficients as follow.

$$\eta_0 = \frac{\rho n^2 D^4 K_T V_a}{2\pi n \rho n^2 D^5 K_Q} = \frac{J K_T}{2\pi K_Q} \tag{2.11}$$

2.2.4. Propeller Open Water (POW) characteristics

The performance characteristics of a propeller is described as Propeller Open Water characteristic, and it is measured using Propeller Open Water equipment installed in a towing tank or a cavitation tunnel as shown in Figure 2.2. The test usually measures the propeller thrust, torque, rotational speed, and water speed together. These results are corrected for water temperature, and in the case of a cavitation tunnel test, the tunnel wall effect is also corrected. Finally, the measurement results are non-dimensionalised using K_T, K_Q, and η, and plotted against J as shown in the Figure 2.1. The open water test procedures recommended by the International Towing Tank Conference (ITTC) can be found in ITTC (2014).

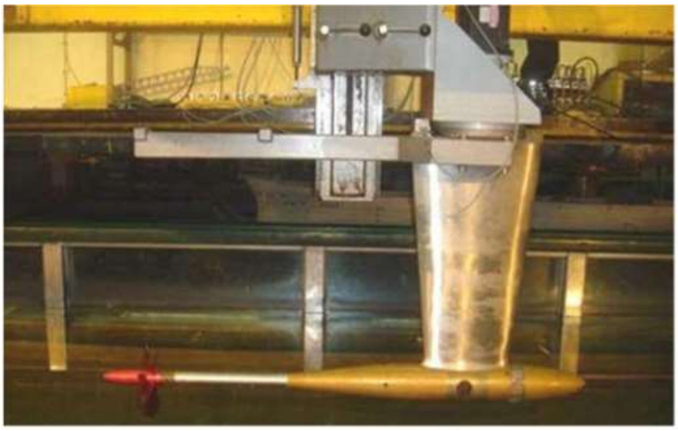

Figure 2.2 The equipment for POW test, adapted from Lim et al. (2014)

2.3. Near-wall flow

2.3.1. Boundary layer

When a viscous fluid passes over an object, the shear stress has a large value only in the thin layer near the object called the boundary layer, and the viscous backflow region is formed by the fluid flowing to the back of the object through the boundary layer. The boundary layer continues to thicken along the length of the object. The flow inside the boundary layer is unstable. It flows smoothly and steadily up to the front part but decomposes into a very unsteady flow at the back of the object.

(a) Laminar flow region: In this region, the boundary layer flow is smooth, orderly, and steady.
(b) Transition region: Here, the smooth flow breaks down.
(c) Turbulent zone: In this region, the flow becomes irregular with random motion, and the boundary layer thickens.

Flow within a turbulent region is described as a superposition of a turbulent velocity component with an average of zero over an average velocity that is constant over time. The random turbulence velocity component is usually on the order of $\pm 20\%$ of the velocity. The turbulent boundary layer also contains a thin viscous sub layer near the surface of the object. Outside the turbulent boundary layer, there is still a smooth, temporally constant external flow, and the turbulent boundary layer is not created because the object is not streamlined. Figure 2.3 shows typical laminar and turbulent flow velocities.

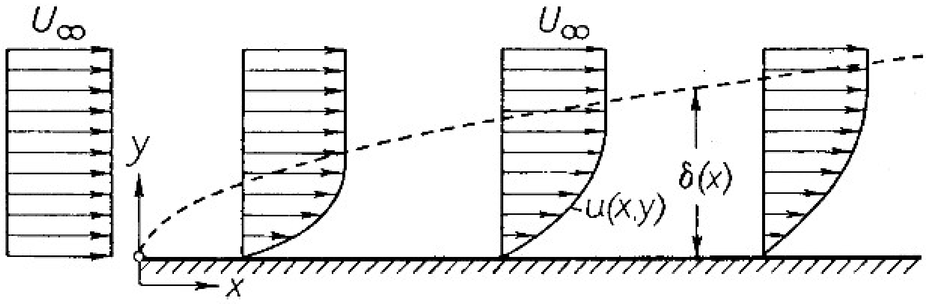

Figure 2.3 Velocity profile of laminar and turbulent flow, adapted from Schlichting (2017)

The initiation of the laminar-turbulent transition process is determined by the velocity of the fluid (v), the distance (l) travelled along the body and the dynamic viscosity (ν) of the fluid. It is characterised by the Reynolds number of the flow defined as follows.

$$Re = \frac{vl}{\nu} \tag{2.12}$$

When Re exceeds about 5×10^5, the flow becomes turbulent even for a smooth shape. At the same time, the laminar-turbulent transition can be promoted depending on the surface conditions, such as surface roughness. The laminar-turbulent transition also depends on the turbulence component already included in the flow approaching the body. Because of ocean waves, tide, shallow water effects, and other local disturbances, ships operate primarily at high levels of turbulent flow. Therefore, the boundary layer around the hull and propeller is turbulent.

2.3.2. Flow Separation

In a fluid flowing along a flat surface, the pressure is constant, and the boundary layer grows thick with distance and does not come off the surface. The case where the pressure decreases in the flow direction is called “the favourable pressure gradient”, but the flow does not separate. On the other hand, the case where the pressure increases in the flow direction is called “an adverse pressure gradient”, and at this time, the flow velocity relatively decreases inside the boundary layer. This causes the velocity of the inner layer of the boundary layer to zero at some point along the length of the object. At that point, the average properties of the boundary layer change dramatically, and the boundary layer thickness begins to get much thicker. The flow at the surface of the body is counter-current, and the main boundary layer is separated from the body, forming a large vortex after the separation point. The separation flow is usually unsteady, with the eddy current periodically falling off into the wake.

Boundary layer separation can occur both laminar and turbulent boundary layers, and it should be noted that it is likely to occur in laminar boundary layers. Looking at the velocity distribution in Figure 2.3, the momentum near the surface of the laminar flow boundary layer is smaller than that of the turbulent boundary layer, which means that the laminar flow boundary layer is more prone to separate. That is, the turbulent boundary layer is more resistant to flow separation than the laminar flow boundary layer. This leads to an increase in drag due to separation in laminar flow rather than turbulence. This fact explains why the dimple-shaped golf ball promotes turbulent flow and thus reduces drag, so it flies farther than the original smooth golf ball.

2.4. CFD

2.4.1. Governing equations

As the governing equations for Newtonian fluid without viscoelasticity, the continuity equation and the Navier-Stokes equation can be expressed. The continuity equation is shown in Equation 2.13 and the Navier-Stokes equation in Equation (2.14). To interpret this numerically, a numerical solution is obtained using CFD.

$$\frac{\partial p}{\partial t} + \nabla \cdot (\rho V) = 0 \tag{2.13}$$

$$\frac{\partial u_i}{\partial t} + u_j \frac{\partial u_i}{\partial x_j} = -\frac{1}{\rho}\frac{\partial p}{\partial x_i} + \frac{\mu}{\rho}\frac{\partial^2 u_i}{\partial x_j \partial x_j} \tag{2.14}$$

A representative numerical technique for simplifying the Navier-Stokes equation is the RANS equation (Reynolds Averaged Navier-Stokes equations). The Navier-Stokes equation can be simplified as Equation 2.15 and Equation 2.16, assuming that the fluctuating velocity and pressure components are divided into the time-averaged value, and the fluctuating part and this process is called the Reynolds average process.

$$\frac{\partial \bar{u}_i}{\partial t} + \bar{u}_j \frac{\partial \bar{u}_i}{\partial x_j} = -\frac{1}{\rho}\frac{\partial \bar{p}}{\partial x_i} + \frac{1}{\rho}\frac{\partial^2}{\partial x_j}\left(\mu \frac{\partial \bar{u}_i}{\partial x_j} - \rho \overline{u_i' u_j'}\right) \tag{2.15}$$

$$\frac{\partial \bar{u}_i}{\partial x_j} = 0 \tag{2.16}$$

$-\rho \overline{u_i' u_j'}$ is the Reynolds stress term

A numerical model is used to solve the RANS equation containing the Reynolds stress term, and representative turbulence models include the $k - \epsilon$ model and the $k - \omega$ model.

2.4.2. Turbulent model

The turbulent viscosity coefficient μ_t is known to be a value determined by the characteristic length and characteristic velocity of the turbulent motion, not by the physical property value from considerations and systematic experiments on turbulence.

The $k - \epsilon$ model is a two-equation model, and the two-equation model is a model that uses the velocity scale and length scale that govern turbulent motion as transport equations. The turbulent kinetic energy (k), which can be obtained directly from the RANS equation, is used as a velocity scale in the form of $(\sqrt{k})$. However, the length scale uses the transport equation for the variable ϵ, which is a combination of the velocity scale and the length scale. ϵ is the dissipation rate of turbulent kinetic energy, expressed as Equation 2.17.

$$\epsilon = \frac{k^{\frac{3}{2}}}{l} \tag{2.17}$$

That is, the $k - \epsilon$ model is a model that calculates the characteristic length by using the turbulent kinetic energy (k) as the characteristic velocity and the dissipation rate (ϵ), and the turbulence viscosity coefficient is expressed as Equation 2.18.

$$\mu_t = \frac{C_\mu \rho k^2}{\epsilon} \tag{2.18}$$

where, C_μ is a coefficient obtained by experiments.

Various $k - \epsilon$ models exist depending on how k and ϵ are constructed to obtain the characteristic length and characteristic velocity. Representative examples include the RNG $k - \epsilon$ model (Yakhot and Orszag, 1986) and Chen's $k - \epsilon$ model (Chen and Kim, 1987). STAR CCM+, a commercial numerical analysis program used in this thesis, includes Standard $k - \epsilon$ Two-layer, Standard $k - \epsilon$ Low-Re, AKN $k - \epsilon$ Low-Re, Realizable $k - \epsilon$, Realizable Two-Layer $k - \epsilon$, etc.

Wilcox (1988) developed the $k - \omega$ model, a model that solves the transport equation of ω, which is the specific dissipation rate (dissipation rate per unit turbulent kinetic energy) instead of ϵ in the $k - \epsilon$ model. The advantage of the $k - \omega$ model compared to the $k - \epsilon$ model is that the performance of the boundary layer is improved in the adverse pressure gradient. However, there is a problem in that the boundary layer calculation is sensitively, changed according to the value of ω in the free stream, and thus there is a disadvantage that it acts extremely sensitively to the inlet boundary condition for the internal flow. In the $k - \omega$ model, the specific dissipation rate and the turbulent viscosity coefficient are calculated as Equations 2.19 and 2.20.

$$\omega = \frac{C_\mu \epsilon}{k} \tag{2.19}$$

$$\mu_t = \frac{\rho k}{\omega} \tag{2.20}$$

where, C_μ is constant.

Menter (1994) developed a method of using the $k - \omega$ model near the wall and the $k - \epsilon$ model in the far-field by introducing the blending function. This method is the SST (shear stress transport) $k - \omega$ model, and this method solves the problem of free stream and inlet conditions, which were disadvantages of the $k - \omega$ model. For this study, the SST $k - \omega$ model is used as the turbulent model.

2.1. Chapter summary and conclusion

A comprehensive review of the literature on related topics, including a high-level understanding and theory of marine propellers, theoretical information on the CFD scheme used in the thesis is presented in this chapter.

3. Methodology

3.1. Introduction

This chapter presents the general methodology used in this thesis, while each of the following chapters will introduce the specific details of the general methodology.

3.2. Approach

Figure 3.1 shows a flow chart of the proposed methodology. Step 1 involves conducting model scale CFD simulations by initially setting the values of wall y+ smaller than 1 and then later greater than 30 on the propeller surface. Step 2 involves validating the model scale simulations by using experimental performance data for the KP505 benchmark propeller of KRISO (Korea Research Institute of Ships and Ocean Engineering). Step 3 involves the simulation of a full-scale propeller initially using low wall y+ and then higher values. The thrust, torque, and efficiency performance of the propellers (in terms of K_T, $10K_Q$, and η_O) were compared with the experimental data and model scale simulations. Step 4 involves CFD simulations using the virtual fluid concept. The full-scale Reynolds number was matched in the model size by using virtual fluid. Finally, the effects of using different values of wall y+ on the propeller surface were investigated based on the various physical characteristics of the propeller performance.

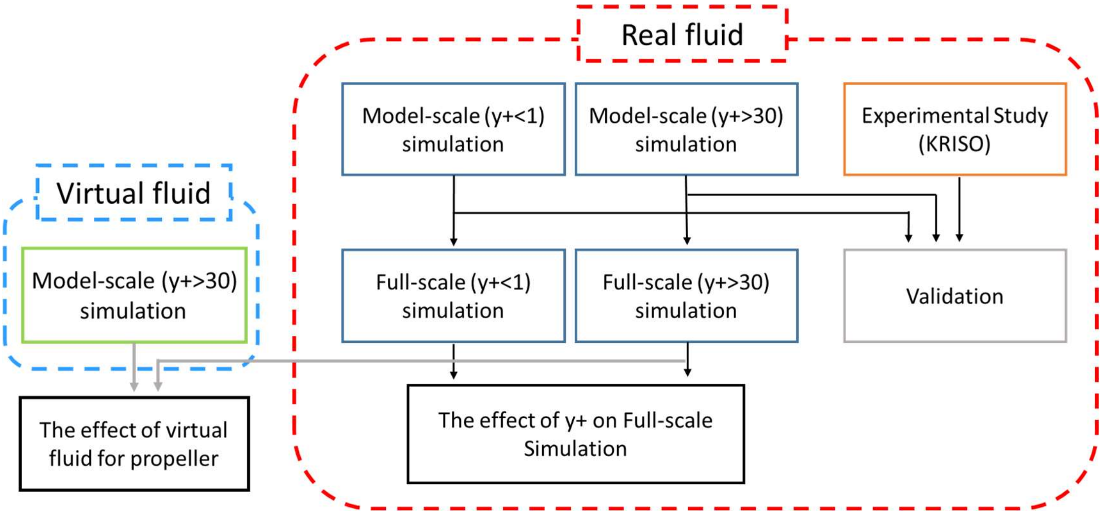

Figure 3.1 The methodology of the whole process

3.3. Mathematical and numerical

3.3.1. Geometry, boundary condition, and grid system

In this thesis, a full-scale and model scale KP505 were used to study the effect of wall y+. The KP505 propeller was designed for the KRISO container ship (KCS). Table 3.1 and Figure 3.2 show the geometry and details of the KP505. The commercial software STAR CCM + 13.06 was used for the analyses conducted in the thesis.

Figure 3.2 shows the grid system used on the propeller surface and surrounding domain of the propeller. At the propeller surface, there is a very fine grid at the propeller tip for better resolution of the tip vortex. The closer to the propeller hub the surface grid is, the larger it becomes. For accurate prediction of the propeller flow, the leading edge and trailing edge were set to have a finer grid. In Figure 3.2, D is the propeller diameter. For the simulations, the sliding mesh method was used. The blue frame shown in Figure 3.2 indicates the rotating region.

Figure 3.3 shows the computational domain and boundary conditions imposed on this domain. The inlet boundary condition is a velocity inlet condition, and the outlet boundary condition is a pressure outlet condition. While the walls have slip conditions, and the propeller surface has a non-slip condition. The fluid flows in the x-direction from the inlet in simulating the advancement of the propeller. To avoid the reflection effects, all boundaries were placed with enough distance from the propeller.

Table 3.1 Main particulars of KP505 propeller

Propeller type		FPP
Rotation		Right Hand
No. of blades		5
Section shape		NACA66
Propeller diameter	D (m)	7.9 (Full), 0.25(Model)
Hub ratio	D_h/D	0.18
Pitch to diameter ratio	P/D	0.950
Blade area ratio	A_e/A_o	0.800

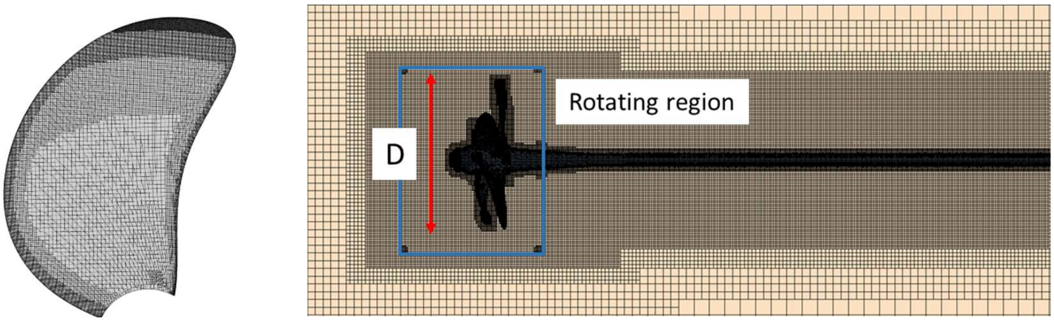

Figure 3.2 Grid system on the propeller surface and volume mesh near the propeller

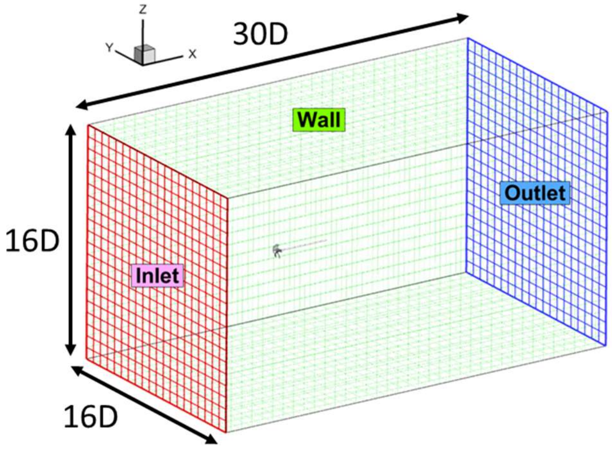

Figure 3.3 Computational domain and boundary conditions

Figure 3.4 shows the prism layer mesh and volume mesh at the $0.7R$ plane of the propeller. The upper edge is the trailing edge, and the lower edge is the leading edge of the blade section. For large wall y+, there is a thick prism layer in Figure 3.4 오류! 참조 원본을 찾을 수 없습니다.(b). All figures have different shapes of the prism layer for each converging condition.

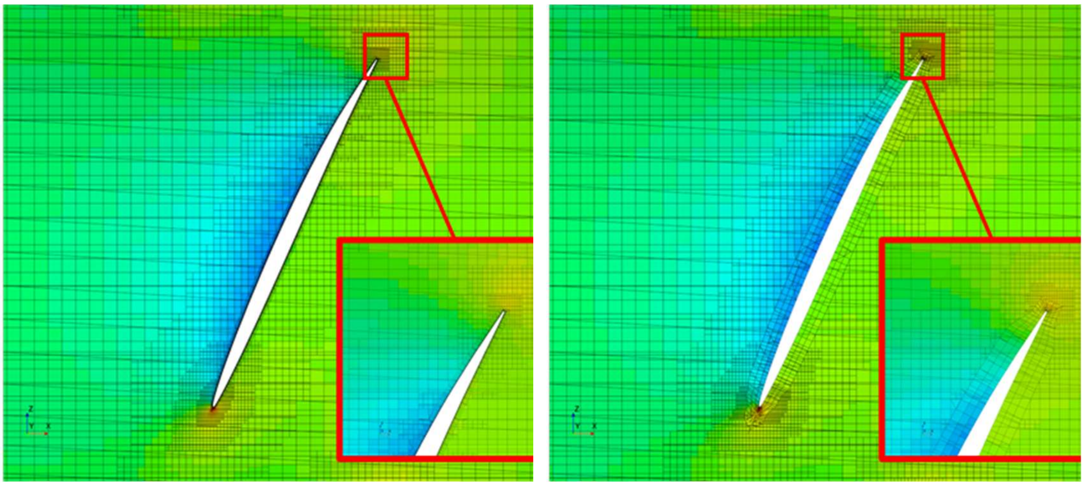

(a) y+<1, model scale

(b) y+>30, model scale

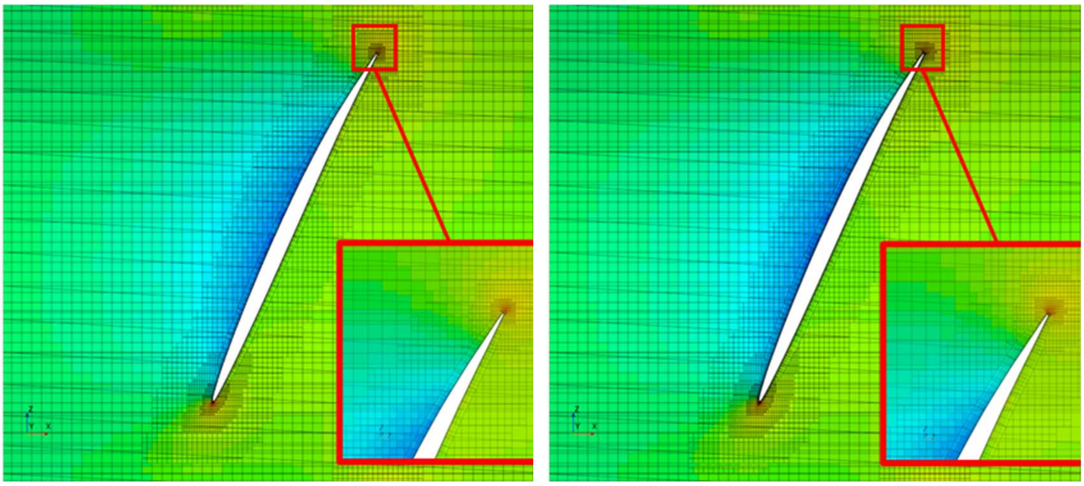
(c) y+<1, full-scale
(d) y+>30, full-scale

Figure 3.4 Prism layer on the propeller blade at 0.7R

3.3.2. Methodology to match small y+ for full-scale simulation

When using CFD, achieving wall y+ less than 1 is one of the biggest challenges in a full-scale simulation due to numerical instability and computing time. To match a wall y+ value less than 1, the prism layer's first cell has to be extremely thin. However, this causes a seriously high aspect ratio, which causes numerical instability. To avoid this situation, the surface grids of the propeller should be very small. In this case, many grid elements are needed. This means that the simulation needs much time to obtain the result. Therefore, researchers must select between numerical stability and computation time.

There are several methods to improve numerical stability. Widely known methods include using a small time step and relaxation factor. For simulations including rotating motion, the numerical instability can be improved by adopting various rotational speeds. After converging numerical conditions are obtained using a stationary propeller, an appropriate rotational speed can be achieved by gradually increasing the rotational speed. But even if these techniques are adopted, these simulations may not converge due to the large aspect ratio. For these reasons, a new technique is needed for the simulation to converge.

When a CFD simulation starts, a constant velocity is used for the initial velocity. This may induce numerical instability at the prism layer because of the high velocity at the layer. To solve this problem, a velocity function with a slope at the wall can be used. This velocity function imitates a boundary layer. It is not needed to express a real boundary layer, and it is just necessary to indicate the virtual boundary layer at the prism layer. By using this artificial boundary layer, the numerical stability can be improved.

An example of how to define the initial velocity condition with an artificial boundary layer is shown by Equation 3.1:

$$\begin{aligned} v &= \frac{v_{\infty}}{t} \times d & \quad (when, d < t) \\ v &= v_{\infty} & \quad (when, d > t) \end{aligned} \tag{3.1}$$

where v is the initial velocity condition, v_{∞} is the inflow velocity, t is the prism layer thickness, d is the wall distance. The slope also can be a second-order, third-order, or logarithm function according to the simulation conditions.

3.4. Chapter summary

The general methodology, including how to set CFD simulations used in the thesis, has been presented in this chapter.

4. Verification and validation

4.1. Introduction

In this chapter, verification and validation of the CFD simulation results were performed by comparing the results with the model experimental data. The grid convergence index (GCI) method was used to verify the grid system of CFD, while for the validation task, the results of the POW test conducted at KRISO were used.

4.2. Verification

To determine the sufficient grid-spacing for the CFD models, a verification study is conducted to assess the numerical uncertainties. The grid convergence index (GCI) method is used to estimate the order of accuracy of results. The GCI method is based on the extrapolation of Richardson (1911).

Table 4.1 shows the GCI values of K_T and K_Q for the full-scale and model scale. N_1, N_2, and N_3 are the numbers of fine, medium, and coarse grids, respectively. The POW characteristics K_T and K_Q at an advance coefficient of $J = 0.5$ were used as the key variables. The difference between the volume mesh base size of the medium-fine grid and the coarse-medium grid is a multiple of the square root of two. However, due to the prism layer, the number of total grids is different by about 2 times.

When doing model scale simulations, the GCI value of K_T and K_Q for the fine mesh arrangement applied was 0.101% and 0.004%, respectively. When doing full-scale simulations, the GCI value of K_T and K_Q for the fine mesh was 0.029% and 0.137%, respectively. There is only a maximum difference of 0.26% between the fine and medium mesh grids. By considering the accuracy and calculation time of simulations, the use of the medium mesh was preferred.

Table 4.1 Comparison of the propeller performance and discretisation error for spatial convergence study

	Model scale			Full-scale		
	No. of grid	K_T(diff., %)	$10K_Q$(diff., %)	No. of grid	K_T(diff., %)	$10K_Q$(diff., %)
N_1 (fine)	18.5 M	0.2724 (-)	0.4354 (-)	39.6 M	0.2866 (-)	0.4251 (-)
N_2 (medium)	9.2 M	0.2717 (0.26)	0.4353 (0.02)	18.4 M	0.2865 (0.03)	0.4260 (0.21)
N_3 (coarse)	5.1 M	0.2718 (0.22)	0.4371 (0.39)	9.3 M	0.2862 (0.14)	0.4269 (0.42)
GCI_{fine}	-	0.101%	0.004%	-	0.029%	0.137%

4.3. Validation

The CFD results were compared with the experimental data from KRISO. Various inflow velocities with a constant shaft rotational speed for all advance coefficients were used for the experiment. The Reynolds number for the propeller can be expressed with the blade chord length and the relative flow velocity at $0.7R$ ($V_{0.7R} = \sqrt{V_A^2 + (0.7\pi nD)^2}$). The Reynolds number for the simulations of the model scale and the full-scale was 8.49×10^5 and 6.22×10^7 at $J_A = 0.7$, respectively.

The comparisons of the predicted POW curves from the CFD with the experimental data are shown in Figure 4.1. The figure on the left, Figure 4.1 (a), illustrates the effect of the different y+ values, while the figure on the right, Figure 4.1 (b), displays the effect of using the different fluid types.

As far as the y+ effect is concerned, the thrust and torque coefficients are in very good agreement with the experimental data as shown (Figure 4.1 (a)) for the different y+ values. The error of η_o is large when the advance coefficient (J) is high. This is because the values of K_T and K_Q are very small at that J range. There are no differences in K_T, K_Q, η_o for the different y+ values in full-scale; whereas at the model scale, the differences can only be seen in K_Q at the high J range.

On the other hand,as shown in Figure 4.1 (b), the result of the virtual fluid agrees well with that of the real fluid, indicating that K_T and $10K_Q$ have similar values at all J values. Thus, the scale effect has not occurred due to the Reynolds similarity.

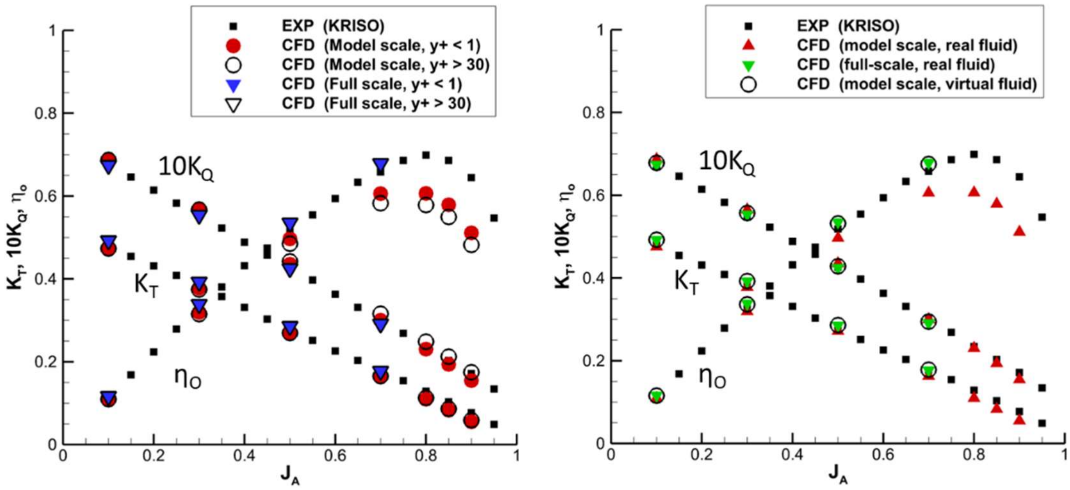

(a) Comparison of effect of the scale and the wall y+

(b) Comparison of effect of the fluid type

Figure 4.1 Propeller open water curves

4.4. Chapter summary

The CFD methods used in this study were verified and validated using the open water performance data for the KRISO benchmark model propeller and the GCI method.

5. Results and discussion

Figure 5.1 and Figure 5.2 show the pressure distributions on the propeller blade surfaces for a low advance coefficient ($J_A = 0.1$) and a high one ($J_A = 0.7$), respectively. For the low advance coefficient case ($J_A = 0.1$), the difference in physical phenomena can be studied in detail by investigating the pressure patterns in Figure 5.1. On the suction side, there are different negative pressure regions at the leading edge. Wall y+ has more effect on the model scale than on the full-scale. For the results of the model scale, the starting point of the strong negative area is located lower when wall y+ is small. Also, the endpoint is located lower. The total areas of the deep blue region are similar to each other. On the other hand, the shape of the negative region is more complex at the lower wall y+ by the split in two at the tip side of the propeller.

Unlike in the model scale, for the full-scale, there is no noticeable difference according to wall y+. The area of the negative pressure region is wider than at the model scale. The starting point is similar to the one with a lower wall y+, and the ending point is similar to the one with a higher wall y+ in the model scale. Because the Reynolds number is the same, the result of the virtual fluid case shows indistinguishable differences from the full-scale results. Both the area and the location of the negative pressure region are similar to the full-scale result, and other areas are similar as well. However, on the pressure side, there are no remarkable differences according to the changes of scale, wall y+ and fluid types. Unlike the suction side, there is a high positive pressure area near the propeller’s leading edge, and a relatively uniform pressure distribution appeared compared with the suction side.

The pressure distribution results for the high advance coefficient ($J_A = 0.7$) is shown in Figure 5.2. The tendency of the pressure contour is dramatically different compared to the low advance coefficient case. Unlike Figure 5.1, there is no difference according to the scale, wall y+, and fluid types. On the suction side of the propeller, a uniform pressure distribution can be seen over the entire surface, and a relatively high pressure distribution can be observed near the trailing edge and the leading edge of the hub side.

Likewise, on the pressure side of the propeller, the contour of the overall pressure distribution is even, and the pressure value is locally high near the leading edge.

The reason for setting a small wall y+ is to set up a thin grid close to the wall for accurately capturing the velocity gradient. On the other hand, a large y + corresponds to the relatively large size that the first grid covers up to the buffer layer. Since the first grid size is large, the overall grid size in the prism layer increases. Eventually, the near-wall grid-resolution quality becomes poor (Figure 3.4).

In the Fluid Volume Method (FVM), one cell has one physical value, so in the case of a large wall y+, the velocity value of the first cell touching the wall has a larger value than when a small y+ is used. Therefore, when the value of wall y+ is large, since the first cell has greater momentum, the area where the flow is separated and negative pressure is generated is biased toward the tip of the propeller. In the case of high Reynolds numbers, however, no tendency appears like at low Reynolds number due to the thin boundary layer.

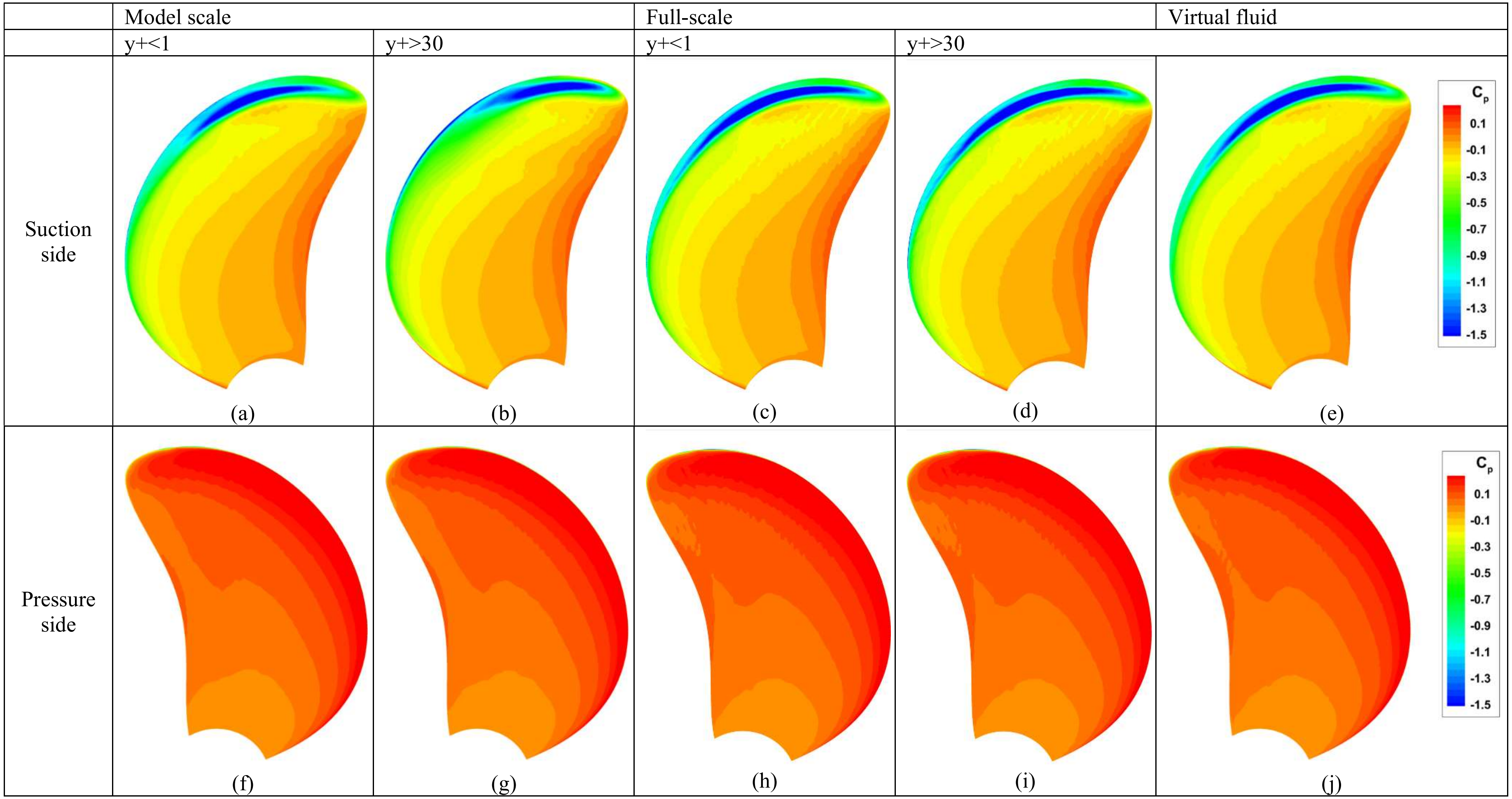

Figure 5.1 Pressure distribution at the propeller surfaces when $J_A = 0.1$

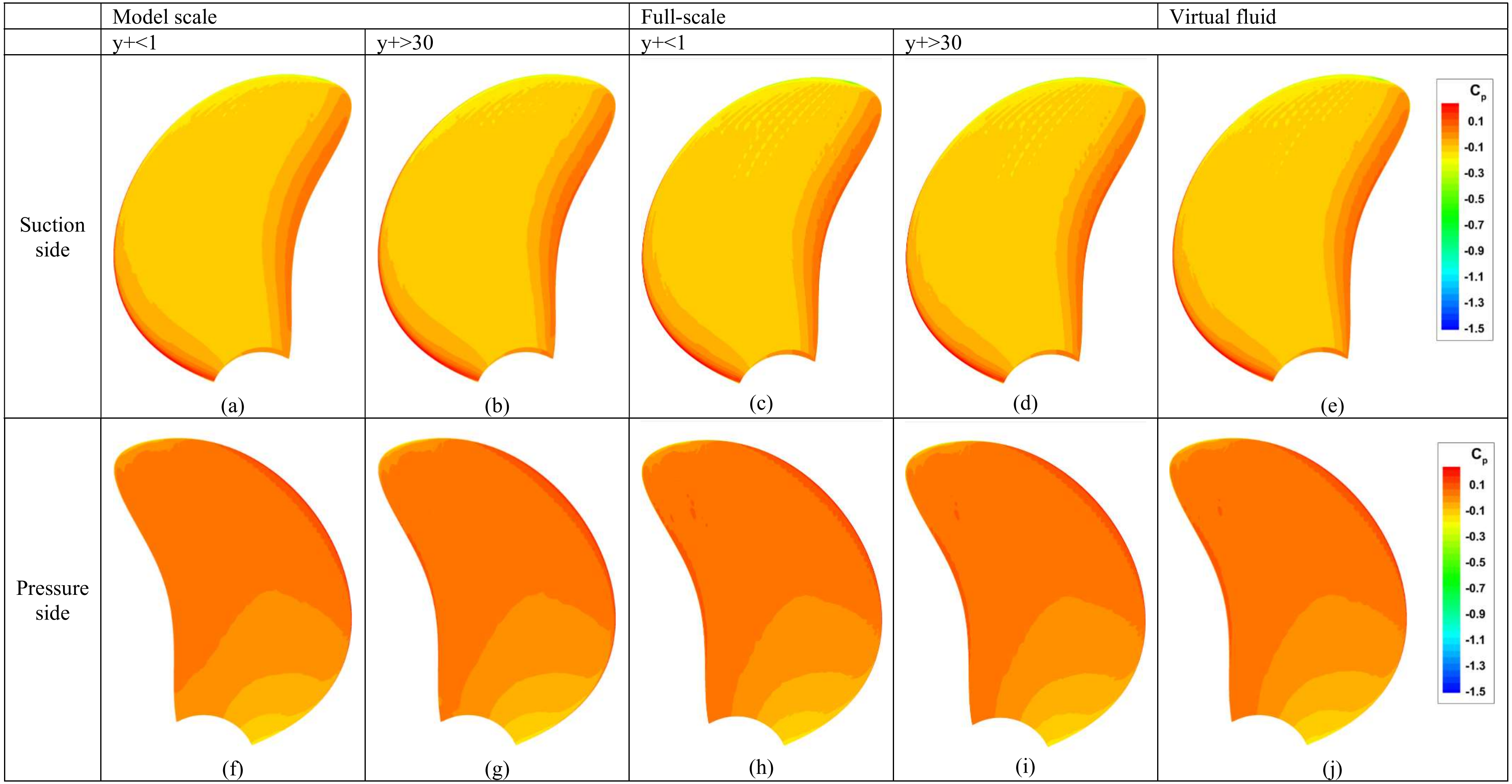

Figure 5.2 Pressure distribution at the propeller surfaces when $J_A = 0.7$

Figure 5.3 shows the friction coefficient and limiting streamline on the propeller blade surface for J_A=0.1. The lines on the blade surfaces represent the limiting streamlines, and the contours represent the friction coefficient distribution. Many differences depend on the scale, and numerical conditions can be discussed. For the low wall y+ value at the model scale, a complex flow appears near the leading edge of the suction side, and the overall shape of the limiting streamlines over the blade is directed toward the propeller tip as the flow progresses. On the other hand, at the high wall y+ value, the complex flow pattern is not observed near the leading edge, and the overall shape of the limiting streamlines over the blade has a concentric circle pattern.

The friction coefficient distribution shows a larger tendency at the high wall y+ value as a whole. Still, a strong friction coefficient appears near the leading edge on the suction side, so the torque coefficient has similar values (i.e. higher torque), as shown in Figure 4.1. In full-scale, there is a different trend compared to the trend observed in the model scale. Because the Reynolds number is much larger, the magnitude of the friction coefficient distribution is smaller than that of the model scale. In addition, there is almost no effect of wall y+ on both the limiting streamlines and contours. The shape of the limiting streamlines is similar to the large wall y+ result of the model scale.

When the advance coefficient is increased (J_A=0.7), as shown in Figure 5.4, there are fewer differences compared to the low advance coefficient (J_A =0.1). For the low wall y+ value at the model scale, the overall shape of the limiting streamlines over the blade is more directed toward the propeller tip as the flow progress than high wall y+. However, the tendency is smaller than the low advance coefficient (Figure 5.3, (a) and (b)). On the other hand, in the Full-scale and virtual fluid results, there is no appreciable difference between the limiting streamlines.

In terms of friction coefficient distribution, similar to the limiting streamline, there is little difference in full-scale simulations. In the model scale, low wall y+, the friction coefficient is higher near the propeller leading edge. The friction resistance is high at the propeller leading edge but gradually decreased as the flow progressed. On the other hand, in the high wall y+, the friction resistance is small at first, then increases in the middle of the surface and decreases again. This tendency does not appeal in the Full-scale and virtual fluid results.

In Figure 5.5, the shape of the limiting streamlines depending on the wall y+ value at the full-scale is compared. The red line represents the streamline at the lower wall y+ value, and the black line represents at higher wall y+ value. As with the model scale results, when the wall y+ is small, the limiting streamline tends to rise toward the tip. However, the difference appears much smaller than the result of the model scale. On both the suction side and the pressure side, it can be seen that the results of the virtual fluid agree well with the results of the full-scale. The complex flow around the propeller tip and the overall limiting streamline agree well, and the friction coefficient distribution on the propeller surface is similar.

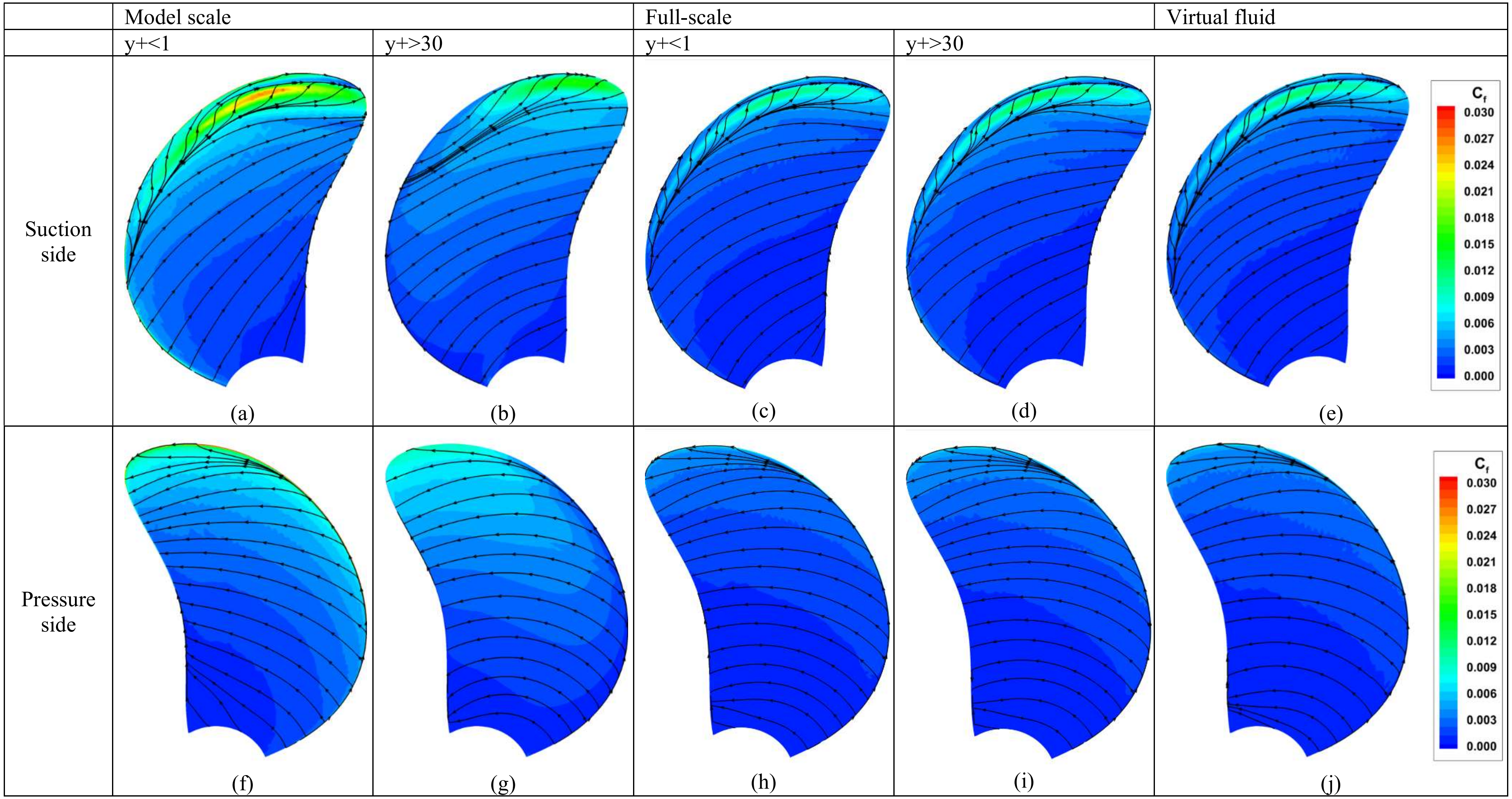

Figure 5.3 Friction coefficient distribution and limiting streamline on the propeller surfaces at $J_A = 0.1$

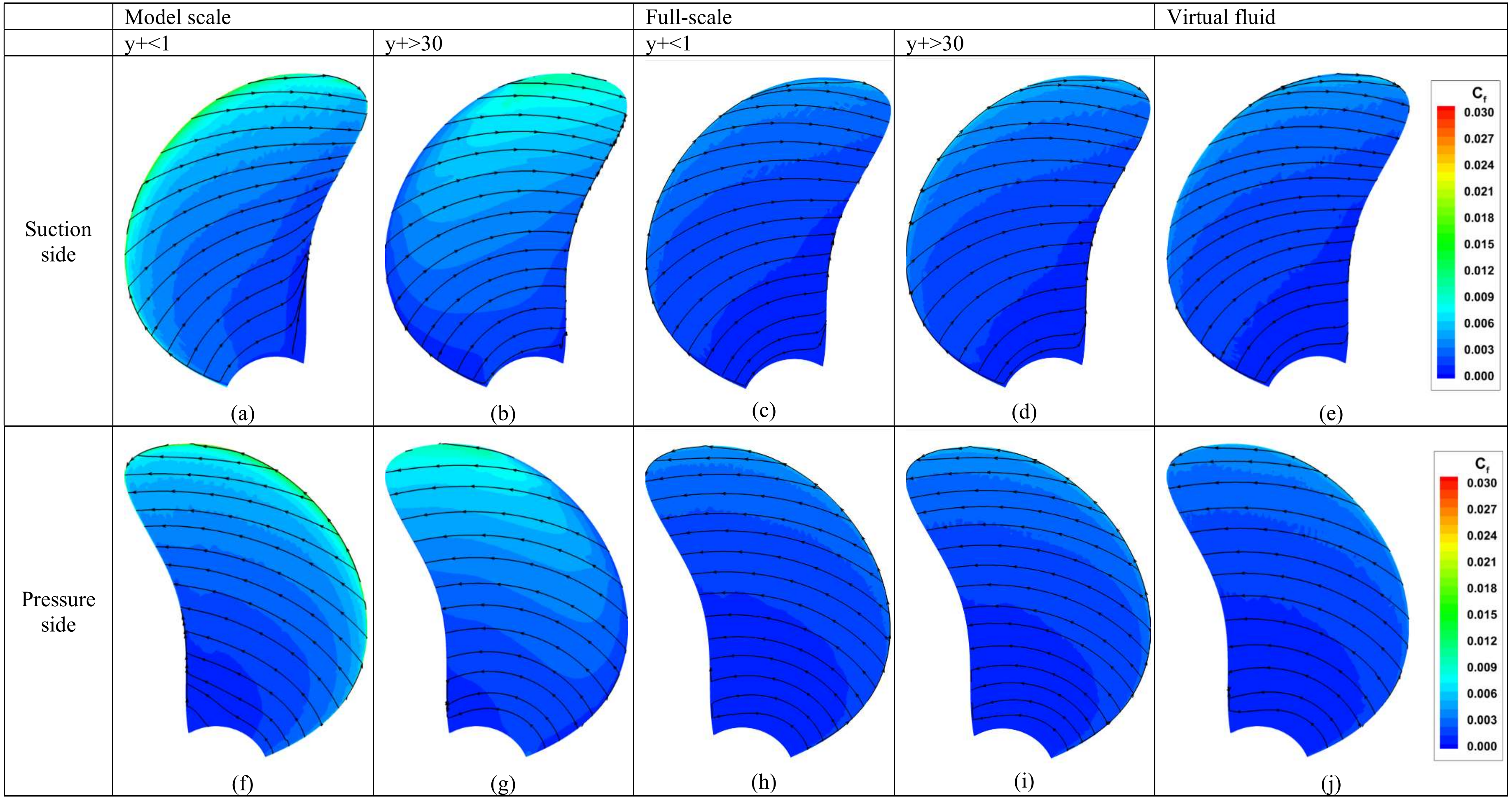

Figure 5.4 Friction coefficient distribution and limiting streamline on the propeller surfaces at $J_A = 0.7$

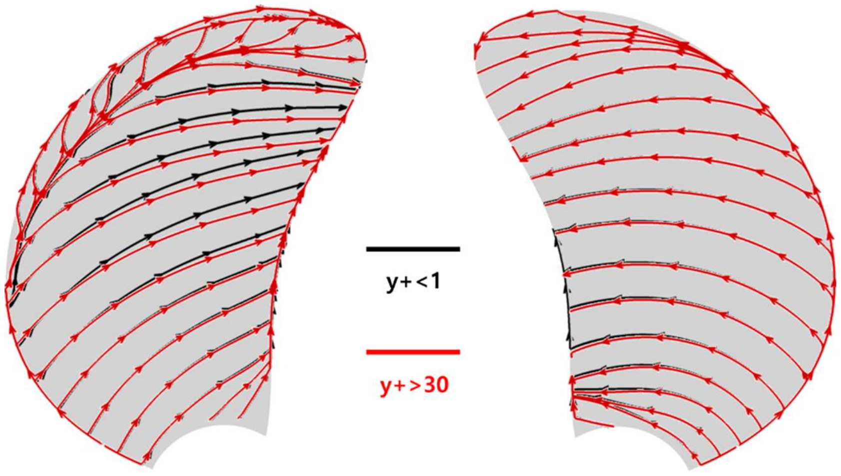

(a) Suction side, $\boldsymbol{J_A} = \mathbf{0.1}$ (b) Pressure side, $\boldsymbol{J_A} = \mathbf{0}.1$

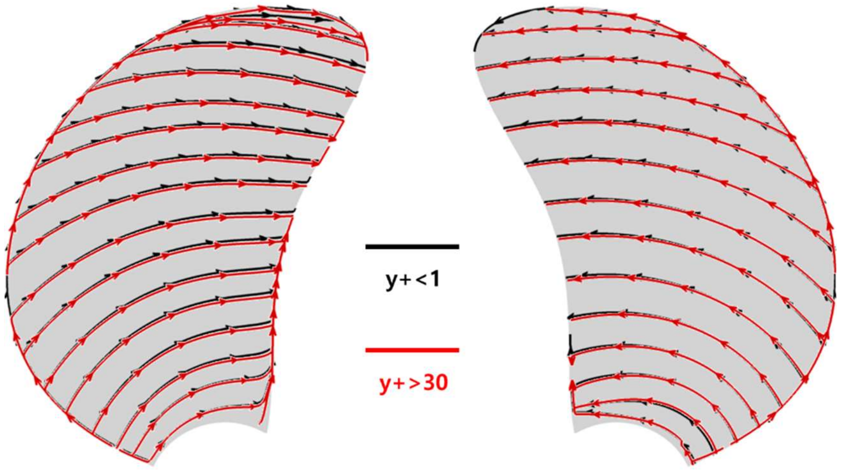

(c) Suction side, $\boldsymbol{J_A} = \mathbf{0}.7$ (d) Pressure side, $\boldsymbol{J_A} = \mathbf{0}.7$

Figure 5.5 The shape of the limiting streamlines on the full-scale propeller surface

Figure 5.6 shows the effect of the y+ value and scale on the pressure field, Q-criteria, friction distribution, and turbulence intensity for the two different advance coefficients. The pressure field near the leading edge of the propeller and the turbulence intensity are plotted based on the Q-criteria. The contours on the blade surfaces represent the friction distribution. Overall, the vortex structure follows the negative pressure region of the pressure field, and the turbulence intensity increases from a similar point. In Figure 5.6 (a) and (b), a difference appears in the vortex structure at the point where the difference appears in pressure distribution (Figure 5.1) and friction distribution (Figure 5.3) on the blade surfaces. A point where the turbulent intensity becomes stronger appears later in Figure 5.6 (b).

The turbulence intensity is a physical quantity that indicates the degree of disturbance of the flow. As mentioned previously, in the case of the large wall y+ value, the momentum of the flow in the first cell is large. For this reason, the disturbance point is behind that obtained with the small wall y+ value. With a low advance coefficient, the results are similar except for Figure 5.6 (b). However, at high Reynolds numbers, the relative thickness of the boundary layer is thin, so the vortex structure adheres more to the propeller surface.

At a high advance coefficient, there is no difference in the physical properties according to calculation conditions. The numerical calculations with the virtual fluid show the results of the full-scale at both the low and high advance coefficients. Both the vortex structure and turbulent intensity are similar. Also, the friction distribution and pressure distribution on the blade surfaces are similar. Therefore, the advance coefficient similarity and Reynolds similarity are correctly applied.

	Model scale		Full-scale		Virtual fluid
	y+<1	y+>30	y+<1	y+>30	
J=0.1	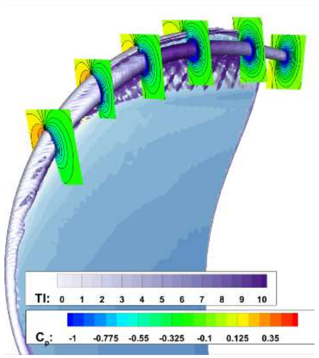 (a)	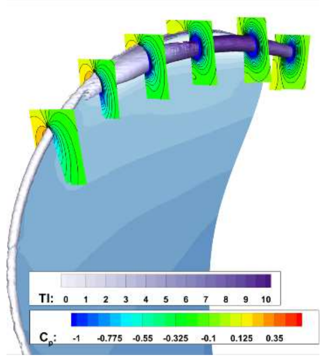 (b)	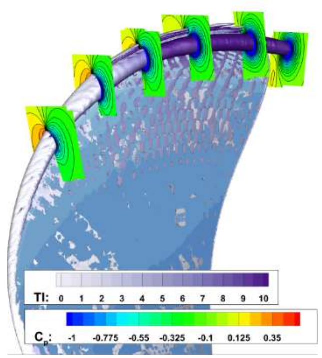 (c)	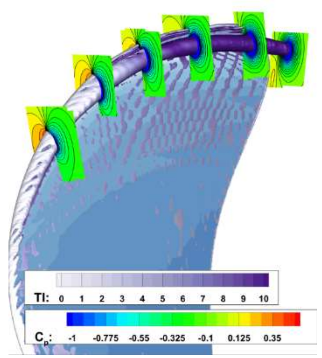 (d)	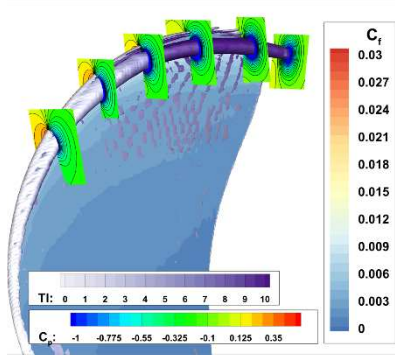 (e)
J=0.7	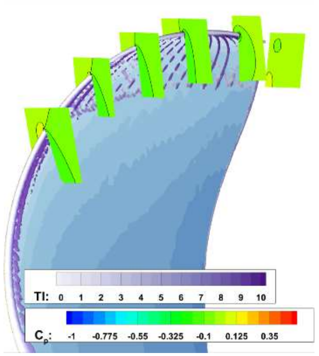 (f)	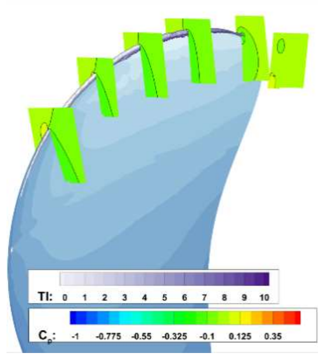 (g)	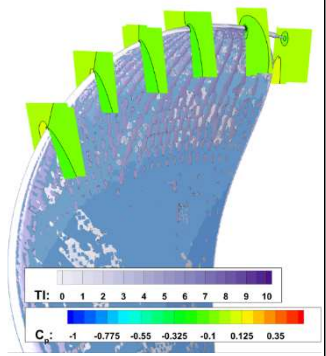 (h)	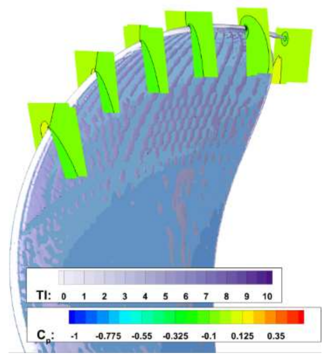 (i)	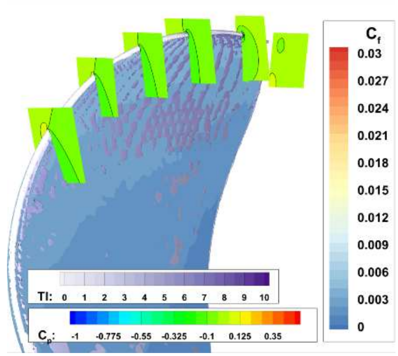 (j)

Figure 5.6 A various physical characteristic on the full-scale propeller

6. Conclusions and recommendations

6.1. Main conclusions

This research investigated the effect of varying wall y+ values and the use of virtual fluid concepts on the prediction of POW performance. During the investigation, the commercial CFD tool STAR CCM+ was used to predict the KRISO KP505 benchmark propeller's POW performance in model and full-scale by using model test data based on a 250-mm-diameter model propeller. Based on the investigations, the following main conclusions were obtained:

- The model scale CFD simulations indicated that the predicted torque coefficient with high wall y+ values overestimated the model test-based torque coefficient at a high advance coefficient ($J_A = 0.7$). However, the agreement for this coefficient was found to be good at a low advance coefficient ($J_A = 0.1$). The thrust coefficient predictions at the model scale were in good agreement with the model-test thrust coefficient at both advance coefficients. However, based on the full-scale simulation results, the CFD predictions overestimated the thrust coefficient in comparison with the predictions from the model scale simulations due to the Reynolds number effect. On the other hand, the predicted full-scale torque coefficient was smaller than the prediction based on the model scale simulations.

- The model scale simulations with the different wall y+ values presented different tip vortex structures and shapes on the blade surfaces. Also, the distributions of the pressure and frictional coefficients were dissimilar, and the limiting streamlines were considerably different due to the wall y+ differences. The limiting streamlines with the low wall y+ value presented the lines directed towards the propeller tip. In contrast, the results with the high wall y+ value presented the limiting streamlines with concentric circles along the propeller radii.

- In general, the results of the full-scale simulations with the different wall y+ values indicated significantly more minor differences in the predicted performance results compared to the results obtained from the model scale simulations. Despite the differences in the wall y+ values, the main performance parameters were similar (i.e., the thrust and torque coefficients, the pressure and friction coefficient distributions, and the vortex structures). The only difference noticed was in the limiting streamline patterns with a slight deviation in the direction. Similar to the observations in the model scale simulations, the direction of the full-scale limiting streamlines with the low wall y+ values were directed towards the propeller tip with a small deviation from the results with the high y+ values.

- For the full-scale simulations with the virtual fluid, the comparative results with the real fluid for K_T, $10K_Q$, and η_o were all in good agreement on the full-scale. There were close similarities in the vortex structures and limiting streamlines near the propeller leading edge between the results of the virtual fluid and those of the real fluid simulations. Both the vortex structure and turbulent intensity were also similar as well as the friction distribution and pressure distribution on the surfaces of the propeller blades. Overall, the results were very similar to the real fluid results of the full-scale simulation.

Based on the main findings of this research, we suggest that the use of small wall y+ value is more important in the model scale simulations than in the full-scale. There was no significant difference between the results based on the different wall y+ values in the full-scale simulation.

More specifically, there is no need to use small wall y+ values for the full-scale simulation except for detailed flow information near the propeller blade surfaces, where small values are important. Even if the detailed surface flow simulations are important, it may be a good alternative to use a wall y+ value of 30 or more when considering the large computing time requirements that may be coupled with some numerical instability problems due to the number of grid elements.

This study also demonstrated that the similarity requirements for the advance coefficient and the Reynolds number could be satisfied simultaneously in the full-scale based on the use of the virtual flow concept in the CFD simulations without any need to conduct full-scale simulations with real fluid.

6.2. Recommendations for future work

Because of the nature of the MPhil degree study and hence scope and time, the study conducted in the thesis is limited. However, during this research study, the author discovered further useful work could be performed on this topic as recommended in the following areas:

- It would be very useful if propeller cavitation analysis will be carried out. Since cavitation analysis must simulate the phase transition of a fluid, a very sophisticated numerical analysis technique must be applied. However, in this study, the cavitation study was not conducted because the numerical instability was too large due to the very small grid size. If propeller cavitation analysis is conducted from the perspective of this study, it will be possible to understand more about the surface damage, performance, and noise problems of propellers.

- In order to accurately estimate the propulsion performance of a ship on the Full-scale, it would be good if the ship's resistance analysis and self-propulsion analysis were verified. Because the advantages of using virtual fluid in propeller analysis have been verified due to this study, if usefulness is verified in resistance and self-propulsion analysis, a new path will be opened for estimating the performance of the ship without performing the Full-scale simulation.

References

Andersen, P. (1999). Tip-Modified Propellers. Oceanic Engineering International, 3(1), 1-11.

Castro, A.M., Carrica, P.M., Stern, F. (2011). Full scale self-propulsion computations using discretized propeller for the KRISO container ship KCS. Computers & fluids, 51, 35-47. https://doi.org/10.1016/j.compfluid.2011.07.005.

Choi, J.-K., Kim, H.-T. (2010). A Study of using Wall Function for Numerical Analysis of High Reynolds Number Turbulent Flow. Journal of the Society of Naval Architects of Korea, 47, 647-655. https://doi.org/10.3744/SNAK.2010.47.5.647.

Dang, J. (2004). Improving cavitation performance with new blade sections for marine propellers. International shipbuilding progress ,51(4), 353-376.

David C. Wilcox. (1988). Turbulence Modeling for CFD, second Ed. D C W Industries

Dyne, G. (2005). On the principles of propellers with endplates. International Journal of Maritime Engineering, 147(3).

Felli M., Camussi, R., Felice, D. (2011). Mechanisms of evolution of the propeller wake in the transition and far fields. Journal of Fluid Mechanics, 682, 5. https://doi.org/10.1017/jfm.2011.150.

ITTC. (2014). ITTC-Recommended procedures and guidelines: Open Water Test.

ITTC. (2011). ITTC-Recommended procedures and guidelines: Practical Guidelines for Ship CFD Applications.

Jasak, H., Vukčević, V., Gatin, I., Lalović, I. (2019). CFD validation and grid sensitivity studies of full scale ship self propulsion. International Journal of Naval Architecture Ocean Engineering, 11, 33-43. https://doi.org/10.1016/j.ijnaoe.2017.12.004.

Kawamura, T., Ouchi, K., Nojiri, T. (2012). Model and full scale CFD analysis of propeller boss cap fins (PBCF). Journal of marine science technology, 17, 469-480. https://doi.org/10.1007/s00773-012-0181-2.

Kim, D.-Y., Ha, J.-Y.,Paik, K,-J. (2020). Numerical Study on the Extrapolation Method for Predicting the Full-scale Resistance of a Ship with an Air Lubrication System. Journal of Ocean engineering and Technology, 34(6), 387-393. https://doi.org/10.26748/KSOE.2020.065.

Lim, S-S, et al. (2014). Parametric study of propeller boss cap fins for container ships. International Journal of Naval Architecture and Ocean Engineering, 6(2), 187-205. https://doi.org/10.2478/IJNAOE-2013-0172.

Menter, F.R. (1994). Two-equation eddy-viscosity turbulence models for engineering applications. AIAA Journal, 32, 1598-1605. https://doi.org/10.2514/3.12149.

Paik, K.-J. (2017). Numerical study on the hydrodynamic characteristics of a propeller operating beneath a free surface. International Journal of Naval Architecture Ocean Engineering, 9, 655-667. https://doi.org/10.1016/j.ijnaoe.2017.02.006.

Richardson, L.F. (1911). IX. The approximate arithmetical solution by finite differences of physical problems involving differential equations, with an application to the stresses in a masonry dam. Philosophical Transactions of the Royal Society of London. Series A, Containing Papers of a Mathematical or Physical Character, 210, 307-357. https://doi.org/10.1098/rsta.1911.0009.

Schlichting, H. (2017). Boundary-Layer Theory (9th Ed.). Berlin Heidelberg: Springer-Verlag.

Sezen, S., Cakici, F. (2019). Numerical Prediction of Total Resistance using Fully Similarity Technique. China Ocean Engineering, 33, 493-502. https://doi.org/10.1007/s13344-019-0047-z.

Siemens. (2018). STAR-CCM+ user guide, version 13.06.

Silvestre, M., Morgado, J., Alves, P., Santos, P., Gamboa, P., Páscoa, J. (2015). Propeller performance measurements at low Reynolds numbers. International Journal of Mechanics, 9, 154-166.

Song, S., Demirel, Y.K., Atlar, M. (2019). An investigation into the effect of biofouling on full-scale propeller performance using CFD. International Conference on Offshore Mechanics and Arctic Engineering American Society of Mechanical Engineers, V002T08A036. https://doi.org/10.1115/OMAE2019-95315.

Yang, H.-U., Kim, B.-N., Yoo, J.-H., Kim, W.-J. (2010). Wake comparison between model and full scale ships using CFD. Journal of the Society of Naval Architects of Korea, 47, 150-162. https://doi.org/10.3744/SNAK.2010.47.2.150.

Zhao, Q., Guo, C., Zhao, D. (2015). Study on self-propulsion experiment of ship model with energy-saving devices based on numerical simulation methods. Ships Offshore Struct, 10, 669–677. https://doi.org/10.1080/17445302.2014.945765.